Ancient midbrain inhibitory neurons control selective spatial attention

Ninad B. Kothari[1], Wen-Kai You[1], Arunima Banerjee[1], Qingcheng Zhang[2], Shreesh P. Mysore[1,2,3,4*]

[1]Department of Psychological and Brain Sciences, Johns Hopkins University; Baltimore MD 21218
[2]Undergraduate Program in Neuroscience, Johns Hopkins University
[3]The Solomon H. Snyder Department of Neuroscience, Johns Hopkins University School of Medicine
[4]Kavli Neuroscience Discovery Institute, Johns Hopkins University
**Corresponding author. Email: mysore@jhu.edu.*

ABSTRACT

The neural circuit mechanisms for the control of selective visuospatial attention remain elusive. Here, in mice, we demonstrate that a relatively unknown, but evolutionarily conserved group of parvalbumin-positive inhibitory neurons in the mammalian midbrain, called the pLTN (periparabigeminal lateral tegmental nucleus), controls target selection and distractor suppression for spatial attention. Selectively inactivating pLTN in mice performing a human-like visuospatial attention task (flanker task) makes mice hyper-distractible, impairing accuracy (and perceptual sensitivity) of the target amidst distractors. It also impairs the reliability (categorical nature) of target selection. These deficits occur without affecting perceptual sensitivity to the target presented singly, motor plan selection, or task-related orienting behaviors. The behavioral results are consistent with pLTN's action on the midbrain sensorimotor hub, the superior colliculus. We thus establish pLTN as a dedicated midbrain seat for the control of selective spatial attention.

INTRODUCTION

The ability to preferentially process information that is most relevant to behavior while ignoring distracting information at all other locations is called selective spatial attention. Critical to adaptive behavior, selective spatial attention is orchestrated by fronto-parietal (*1, 2*) and midbrain (*3, 4*) networks. Although damage to these networks in human patients, and their selective inactivation in non-human primates (*5, 6*), causes deficits in spatial attention, what specific mechanistic loci within them implement distracter suppression and target selection (and how they do so) is not understood.

Converging evidence from recent studies of the evolutionarily conserved vertebrate midbrain has spurred an intriguing hypothesis. Focal inactivation of the midbrain sensorimotor hub, the superior colliculus (SC), and specifically, its intermediate and deep layers (SCid), in behaving monkeys disrupts selective spatial attention (*5, 6*). The resulting attentional deficits occur only when the target is present amidst task-relevant distracters (but not when it is alone). These results revealed that competitive interactions among stimulus representations within SCid, which encodes a topographic map of sensory and motor spatial locations, are critical for selective spatial attention (*7*). In parallel, work in passive birds has revealed that a group of parvalbumin-positive midbrain inhibitory neurons, called nucleus isthmi pars magnocellularis (Imc) (*3, 8*), controls competitive interactions within the OTid space map (avian analog of SCid; (*9*)). These neurons, which are bidirectionally connected with the OT, are thought to be conserved across vertebrates (*10-13*), and are referred to in mammals as the periparabigeminal lateral tegmental nucleus (pLTN) (*10*). Together, these past results have led to the hypothesis that pLTN/Imc may play a critical role in selective spatial attention in vertebrates (*3, 10, 12, 14*). However, the contribution of pLTN

neurons to adaptive behavior has never been studied in any vertebrate species (nor has its contributions to SCid processing in mammals). Here, with anatomical, electrophysiological and behavioral experiments, we first identify pLTN in mice and then establish it as a midbrain seat for attentional control, orchestrating distracter suppression and categorical target selection for selective spatial attention.

RESULTS

To identify candidate inhibitory pLTN neurons in the mouse midbrain tegmentum, we first visualized GABAergic neurons near the parabigeminal area (*15*), inspired by previous work in cats and ferrets (*10, 12, 16, 17*) (Fig. 1A left). Midbrain sections from a wild-type mouse, immunostained for GABA, showed that labeled GABAergic neurons were distributed across the parabigeminal nucleus (PBG) and the neighboring microcellular tegmental nucleus (MiTg/pLTN; see methods; Fig. 1A middle). Co-immunostaining for parvalbumin (PV) in these sections showed that nearly all GABA+ neurons exhibited co-labeling for PV (Fig. 1A-right, 95.82% GABA+ neurons overlapped with PV immunostained cells, and 93.33% PV+ neurons overlapped with GABA immunostained cells) making these GABAergic PV+ neurons, collectively, a candidate for pLTN in the mouse. To examine the connectivity of these PV+ GABAergic neurons with the SC, we first injected a fluorescent tracer (Dextran; see methods) focally into the SC of a PV-tdTomato mouse (Fig. 1B left, middle, see methods), and found anterogradely labeled projections surrounding these PV+ neurons (Fig. 1B-right). Next, we injected a cre-dependent AAV vector expressing eGFP in PBG/MiTg area of PV-Cre mice (60 nL; AP-4.30; ML+1.75; DV-3.5; Fig. 1C, left and middle) and found anterogradely labeled projections in the intermediate and deep layers of the SC (Fig. 1C, right). Thus, PV+ GABAergic neurons in the mouse midbrain lateral tegmentum receive inputs from the SC and send long-range outputs to the SCid. Together, these results established that PV+ GABAergic neurons in the PBG/MiTg midbrain area constitute the pLTN in the mouse.

To test if these pLTN neurons functionally inhibit SCid activity, we activated them chemogenetically (by stereotaxically injecting cre-dependent AAV expressing the excitatory DREADD (AAV.DIO.hM3D(Gq)) in PV-Cre mice, see Methods, Fig. 1D left), and recorded extracellular neural activity simultaneously both of these neurons and of those in SCid in passive mice. CNO administration demonstrated that pLTN neurons inhibit spontaneous activity in SCid (Fig. 1D middle and right).

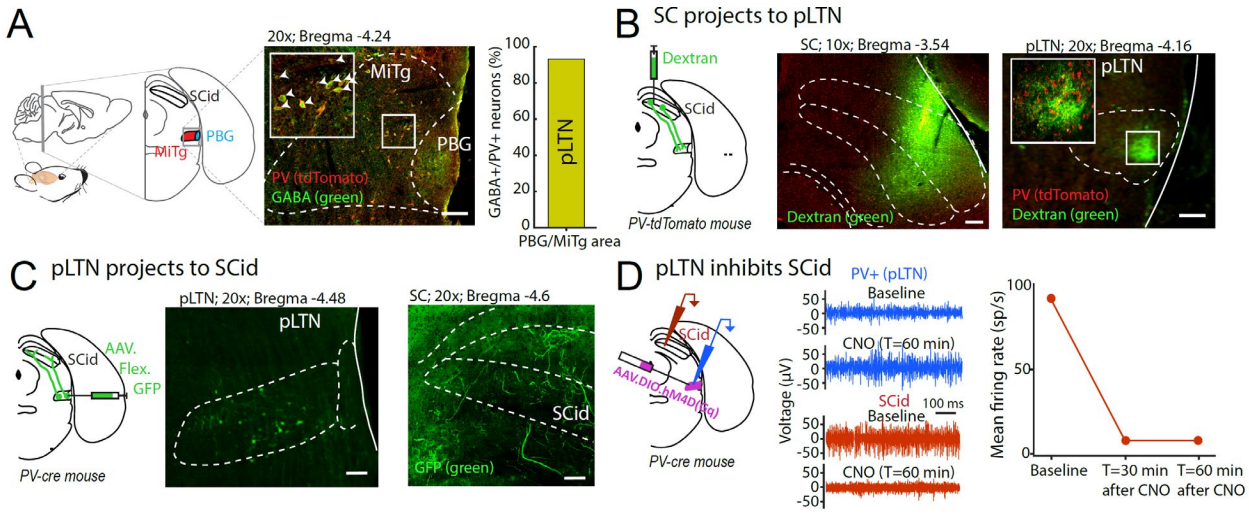

Fig. 1. pLTN neurons in mice are PV+ GABAergic neurons in midbrain lateral tegmentum that are bidirectionalyl connected with the SC. ***(A)*** *Anatomical location of mouse MiTg/PBG area and colocalization of GABA+/PV+ cells. (Left) Anatomical location of MiTg/PBG area based on mouse atlas. (middle) immunohistological labeling of GABA+ (green) and PV+ (red) cells near the MiTg/PBG area.*

Dotted line shows the putative location of pLTN. (inset) A zoomed in image of colocalized GABA+/PV+ cells. Colocalized cells are indicated by white arrows. (right) Summary of percentage of GABA+/PV+ colocalized cells across right pLTN of one wildtype mouse. ***(B)*** *SC projects to pLTN. (left) Schematic showing a Dextran (green) injection in SCid and projection of axons to the putative pLTN of a PV-tdTomato mouse. (middle) injection site (Dextran) in the SCid. Dotted white lines showing location of SCid in a representative section. (right) Dense projection fibers (green) in the putative pLTN area (white dotted lines). (inset) shows a zoomed region (indicated by white square) with projection fibers (green) and PV+ cells (red).* ***(C)*** *pLTN projects to SCid. (left) Schematic shown location of AAV.Flex.GFP injection (green) in the pLTN area and projection fibers in the SCid of a PV-Cre mouse. (middle) PV+ labeled cells (green) at the injection site in the pLTN area (white dotted lines). (right) Projection fibers (green) in the SCid (white dotted lines).* ***(D)*** *pLTN functionally inhibits SCid. (left) Schematic showing location of excitatory DREADD (AAV.DIO.hM3D(Gq)) injection (pink) in a PV-Cre mouse and locations of silicon probes for electrophysiologically simultaneously recording extracellular activity in the pLTN (blue) and SCid (red). (middle) Bandpass filtered extracellular activity for baseline and 60 minutes after CNO injection (i.p.), in the pLTN (top, blue) and SCid (bottom, red). (right) Mean activity of isolated units (n=30, one mouse) in the SCid over the course of 60 minutes after CNO injection (baseline activity recorded 5 minutes before CNO injection). All scale bars are 100 um.*

We next tested if pLTN neurons control competitive stimulus interactions in SCid. To this end, we first characterized competitive interactions in SCid, and then examined the effects of silencing the PV+ inhibitory neurons on these interactions (see methods; (*3, 9, 18-20*)). We performed extracellular recordings in SCid of head-fixed mice passively viewing two stimuli whose relative strength was varied systematically (*19, 21*): one stimulus, S_{in}, a looming dot of fixed strength (loom speed), was displayed within the spatial receptive field (RF) of the SCid neuron, typically in the binocular field (Fig. 2A-top, 2B, 2C-leftmost panel), while a second, competing stimulus, S_{out}, of varying strength was presented in the periphery, far outside the RF (Fig. 2A-top, Fig. 2C-left, see Methods). The resulting responses are referred to as competitor strength-dependent response profiles (*19, 21*). We found that SCid competitor strength-dependent response profiles are similar to those reported in bird OTid (*19*). The responses decreased with S_{out} strength (Fig. 2C-black raster and black data points, showing a negative correlation with the strength of S_{out}; average correlation across 14 sites; see Methods), and were well fit by a sigmoidal curve (Fig. 2C-black curve, see Methods). These results demonstrated a progressive increase in suppression of SCid responses to S_{in} by the distant competing S_{out} of increasing strength.

Published studies have revealed that silencing Imc in birds severely disrupts competitive interactions and competitor-strength dependent response profiles in OTid, with three specific signatures predicted for bilateral silencing: (i) an overall increase in stimulus evoked responses, due to disinhibition of OTid neurons following inactivation of tonic GABAergic inputs from high-firing Imc neurons (*3, 9, 18, 20*), (ii) a much weaker S_{out} strength needed to powerfully suppress SCid responses to S_{in}, due to loss of long-range competitive inhibition by Imc and imbalance in stimulus competition (*9, 18*), and (iii) more gradual (less categorical) OTid response profiles, due to the loss of specially organized competitive inhibition from Imc neurons (*22, 23*).

We reasoned, therefore, that should pLTN in the mouse midbrain function similarly to Imc in the bird midbrain, then bilaterally silencing them should recapitulate all three signature effects in SCid responses. To test this, we stereotaxically injected cre-dependent AAV expressing the inhibitory DREADD (AAV.DIO.hM4D(Gi)) bilaterally in PV-Cre mice (Fig. 2A, see Methods). Strikingly, upon CNO administration, we found all three effects. Compared to SCid responses in the intact case: (i) there was a net upward shift (increase) in stimulus evoked SCid firing rates (Fig. 2D), (ii) there was an additional leftward shift of the SCid response profile, indicating that a weaker S_{out} was indeed sufficient to powerfully suppress responses to S_{in} (Fig 2E), and (iii) the response profiles were less categorical (Fig. 2F; see Methods). These effects on SCid responses were due to CNO-dependent silencing of the PV+ GABAergic neurons in the midbrain tegmentum, because repeating SCid measurements with saline administration had no effect. Taken together, the above

results established that mouse pLTN is functionally analogous to the lmc in non-mammals, and that it shapes long-range competitive stimulus interactions in the SCid.

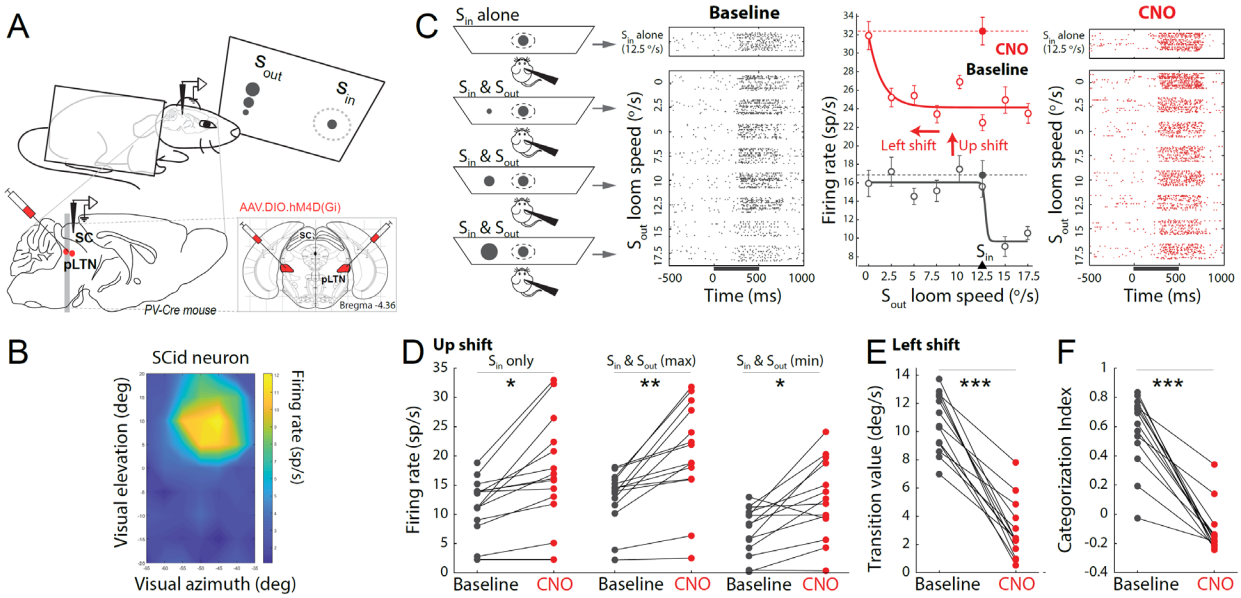

Fig. 2. Bilateral pLTN inactivation disrupts competitive interactions in the SCid. ***(A)*** *Extracellular recordings in a passive head-fixed mouse SCid and bilateral chemogenetic pLTN inactivation. (top) Schematic of electrophysiological recordings in mouse SCid in passive mouse viewing two competing stimuli. (bottom) Schematic showing location of inhibitory DREADD virus (AAV.DIO.hM3D(Gq)) in the pLTN (red; both sagittal and coronal sections) in a PV-Cre mouse.* ***(B)*** *Example 2D receptive field of SCid neuron.* ***(C)*** *Disruption of competitive interactions in the SC by pLTN inactivation. (left) Schematic of experimental protocol for characterizing competitive interactions with two competing stimuli (S_{in} – receptive field stimulus and S_{out} – competing peripheral stimulus). (black and red raster plots) Raster plots of an example SCid neuron in control condition (black raster) and with bilateral pLTN inactivation (red raster). In each raster, top raster panel is when S_{in} alone is present, bottom panel – when both S_{in} and S_{out} are present and with loom speed of S_{out} parametrically varied. Stimulus presentation is shown by gray line along the x-axis. (middle) Competitor response profiles of same SCid unit as shown in adjacent raster plots (black and red). Open circles are firing rates of S_{in} neuron at different S_{out} loom speeds (mean +/- sem), black in control condition and red with pLTN inactivation (CNO). Solid lines (black and red) are corresponding sigmoid fits. Black arrow on x-axis indicates when S_{in} and S_{out} loom speeds were equal. Dashed black and red dashed lines indicate mean firing rate when S_{in} alone was presented in each condition. Red arrows indicate upward and left ward shifts of the competitive response profile for visualization.* ***(D)*** *Mean firing rates of 14 isolated SCid neurons across the baseline (black) and CNO (red) conditions. (left) When S_{in} alone is present (middle and right), the max and min sigmoidal fits when both S_{in} and S_{out} are present.* ***(E)*** *Transition values obtained from sigmoid fits in each condition.* ***(F)*** *Categorization index values obtained across conditions.*

We next tested pLTN's role in the control of selective spatial attention. We trained freely behaving mice on a modified version of a touchscreen-based task of spatial attention (Fig. 3AB, (*24*)), modeled directly after the classic flanker task of attention in humans (*25, 26*). Mice were trained to report the orientation of a central visual target (vertical or horizontal grating) of fixed contrast, while simultaneously ignoring a flanking distracter (also a grating) whose contrast was parametrically varied (Fig. 3B). They were rewarded for correctly reporting a vertical (horizontal) target with a nose-touch within the lower (upper) response port (Fig. 3B). This task design allowed the dissociation of the locus of selective spatial attention (central or peripheral location) from the locus of behavioral report (upper or lower location). There were three task conditions: (a) *Target only condition*, in which the flanker is absent, (b) *Congruent-flanker condition*, in which the target and flanker orientations have the same orientation, and (c) *Incongruent-flanker condition*, in which

the target and flanker have opposite orientations (Fig. 3B). All conditions and distractor contrast levels were pseudo-randomly interleaved (see Methods).

Consistent with previously published results in humans (*25, 26*) and in mice (*24*), the overall performance (across flanker contrasts) was high for the target-only and congruent-flanker conditions (high accuracy and fast reaction times), but was significantly lower for the incongruent-flanker task (lower accuracy and longer reaction times – T-alone vs congruent trials, $p=0.77$, signed-rank test; congruent vs incongruent trials, $p<0.05$, signed rank test; Fig. 3C). Human studies with the flanker task also indicate that incongruent trials with low flanker-contrasts, in which attention is driven to the target location by top-down expectation of reward, represent the 'attend-towards' target condition, whereas incongruent trials with high flanker-contrasts, in which the top-down expectation is overwhelmed, and attention captured by, the salient flanker, represent the 'attend-away' from target condition (*26-28*). We found significantly higher target selection performance (w.r.to accuracy) in attend-towards trials (trials with the two lowest flanker contrast) compared to attend-away trials (trials with the two highest flanker contrasts) (Fig. 3D), revealing classic signatures of spatial selective attention in mice in this task. Finally, unpacking performance in the incongruent-condition as a function of flanker contrast, we found that psychometric curves of attentional target selection exhibited an large, abrupt drop in performance when flanker contrast just exceeded that of the target (*24*) (Fig. 3E).

To test pLTN's role in spatial attention, we next trained PV-cre mice on the flanker task and then stereotaxically injected cre-dependent AAV expressing the inhibitory DREADD, bilaterally into pLTN (see Methods, n=7 PV-cre mice; see methods, Fig. 3FG, Fig. S4). Following 3 weeks of expression, we compared the effects of CNO vs. saline administration on behavioral performance in the spatial attention task. We found that whereas overall performance (% correct) was not different in the congruent flanker condition between saline and CNO administration, overall performance in the incongruent condition significantly dropped following CNO (Fig. 3H, red vs. teal data, no-flanker condition, $p=0.26$, signed-rank test; incongruent condition, $p<0.01$, signed-rank test). Additionally, performance in attend-towards trials dropped dramatically following CNO administration (Fig. 3I). Notably, unpacking the effect of CNO on performance as a function of flanker contrast revealed several striking findings. In the incongruent flanker condition, (a) The psychometric curve was shifted leftward such that even weak distractors were sufficient to powerfully impair behavioral responses to the target (Fig. 3J, black asterisk: $p < 0.05$; incongruent CNO trials at given contrast (red) were significantly different from incongruent saline trials at same contrast, signed-rank test); (b) Performance when the distractor was stronger than the target also deteriorated (Fig. 3J, black asterisk: $p < 0.05$; incongruent CNO trials at given contrast (red) were significantly different from incongruent saline trials at same contrast, signed-rank test); and (c) The psychometric curve of attentional target selection became substantially less categorical nature (Fig. 3J and S4). By contrast, in the congruent condition, (d) performance and sensitivity were intact across distractor contrasts. We tested if the results in the incongruent condition could be due to non-specific (DREADD-independent) effects of CNO by repeating these experiments with WT mice expressing a control virus (AAV.FLEX.GFP; n=3 WT mice; see Methods). We were able to rule out this alternative possibility because we found no impact of CNO on performance in the incongruent-flanker condition (Fig. S4). Finally, we found an increase in reaction times with pLTN inactivation across the three conditions (Fig. 3H-right, red vs teal; congruent, $p<0.05$, signed-rank test; incongruent, $p<0.05$, signed-rank test).

Together, these results established that bilateral silencing of pLTN causes hyper-distractibility (an ADHD-like deficit) and loss of categorical target selection in mice.

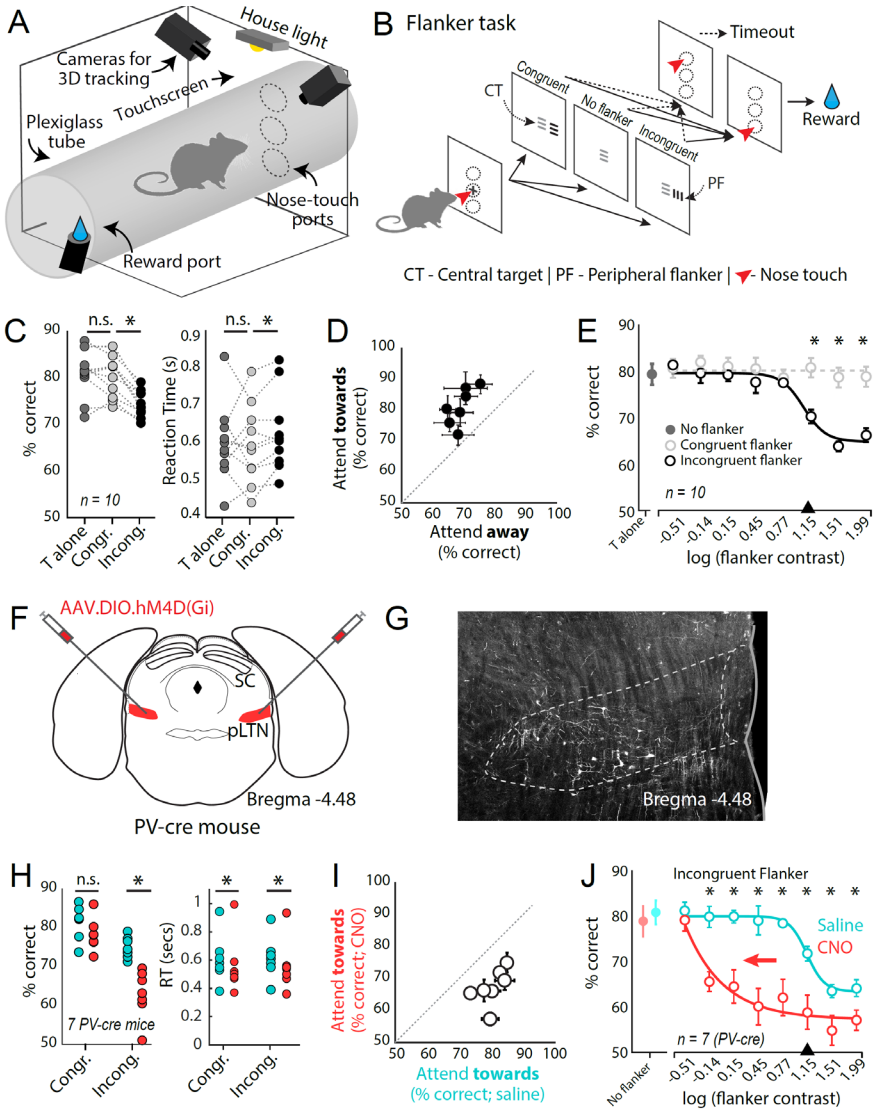

Fig. 3. Bilateral pLTN inactivation disrupts target selection and distractor suppression for selective spatial attention. *(A) Schematic of touchscreen-based mouse behavior setup.* ***(B)*** *Schematic of task design.* ***(C)*** *Comparison of task parameters across the target-alone, congruent and incongruent task conditions for 10 mice. (Left) Mean percentage correct, (right) Median RT. Each dot represents data from one mouse. Dotted lines connect mouse task parameters across condition.* ***(D)*** *Percentage correct (mean +/- sem) in the attend-toward and attend-away conditions.* ***(E)*** *Percentage correct across flanker contrasts, for congruent condition (open light-gray circles, mean +/-sem) and incongruent condition (open black circles, , mean +/-sem). Black solid line is sigmoid fit to the incongruent data. Closed circle are for target only trials. Black arrow on x-axis indicates when target and flanker contrasts are equal. Dashed light gray line indicates mean performance across flanker contrasts for congruent trials.* ***(F)*** *Schematic showing location of bilateral inhibitory DREADDs injection in the pLTN.* ***(G)*** *Image showing labelled pLTN cells (white – tdTomato) with chemogenetic virus.* ***(H)*** *Comparison of task parameters across the saline and CNO conditions for congruent and incongruent task conditions for 7 PV-Cre mice. (Left) Mean percentage correct, (right) Median RT. Each dot represents data from one mouse.* ***(I)*** *Comparison of percentage correct (mean +/- sem) for the Saline and CNO conditions in the attend-toward conditions.* ***(J)*** *Percentage correct across flanker contrasts, for incongruent condition with saline (open cyan circles, mean +/-sem) and CNO (open red circles, mean +/-sem). Corresponding solid lines are sigmoid fits. Closed circles are for target only trials. Black arrow on x-axis indicates when target and flanker contrasts are equal.*

Are these deficits in behavior following bilateral silencing of pLTN due to impairment of attentional selection, or could they be explained by alternative causes? Considering the connectivity of pLTN with the SCid, a well-established sensorimotor structure, three alternatives are possible – motor plan selection deficits, visual perceptual deficits, or motor execution (orienting) deficits.

First, we considered potential motor plan selection deficits. Inactivating the pLTN could disrupt selection among motor plans to respond at the upper versus lower response ports, rather than disrupting attentional target selection, and manifest as impairments in performance accuracy. We ruled this out because of the design of our task in which the locations of the competing attentional targets (central versus peripheral) are dissociated from those of the behavioral responses (up vs. down). Thus, potential impairments in motor plan selection would be unable to account for the observed behavioral results.

Second, we investigated potential perceptual deficits following pLTN silencing. Inactivating the pLTN could cause a deficit in visual perception (*5, 29*) which can account for the decrease in performance accuracy and perceptual sensitivity. To address this, we examined the behavioral responses in the no-flanker condition of the flanker task, and found that CNO administration did not alter performance accuracy, (although reaction times were faster) compared to saline administration (Fig. 4A; red vs teal; congruent, $p<0.05$, signed-rank test). As an additional test, we tested PV-cre mice (n=4; with bilateral inhibitory DREADD injected in the pLTN; Fig. 3, see methods) on single target discrimination task, essentially, the no-flanker condition in the flanker task, but with one exception: we systematically varied the contrast of the target. Interestingly, we found no difference in single-target performance between the CNO and saline administration conditions (Fig. 4B). These results indicated that pLTN silencing did not produce any visual perceptual deficits.

Third, we investigated potential motor execution deficits following pLTN inactivation. Inactivating the pLTN could cause a deficit in task-related orienting behaviors appearing as impairments in performance accuracy. To address this, we tracked the head-orienting movements of the mice in 3-dimensions (Fig. 4C), while they performed the flanker task, using calibrated video cameras (Fig. 3A; see Methods). We found no difference between the CNO and saline conditions, in movement trajectories (Fig. 4D), in 3D head displacement (Fig. 4E), or in 3D head direction during touchscreen interaction in trials (Fig. 4F). Together with the recent report that mice only infrequently make independent eye saccades (eye-in-head orienting) during goal directed tasks, but rather, predominantly make head-orienting movements to acquire targets (*30*), our results establish that task-relevant gaze and orienting movements are largely unaffected by CNO administration. Thus, we were able to rule out alternative explanations for the observed behavioral deficits following bilateral pLTN inactivation, and conclude that pLTN silencing disrupts attentional target selection for spatial attention.

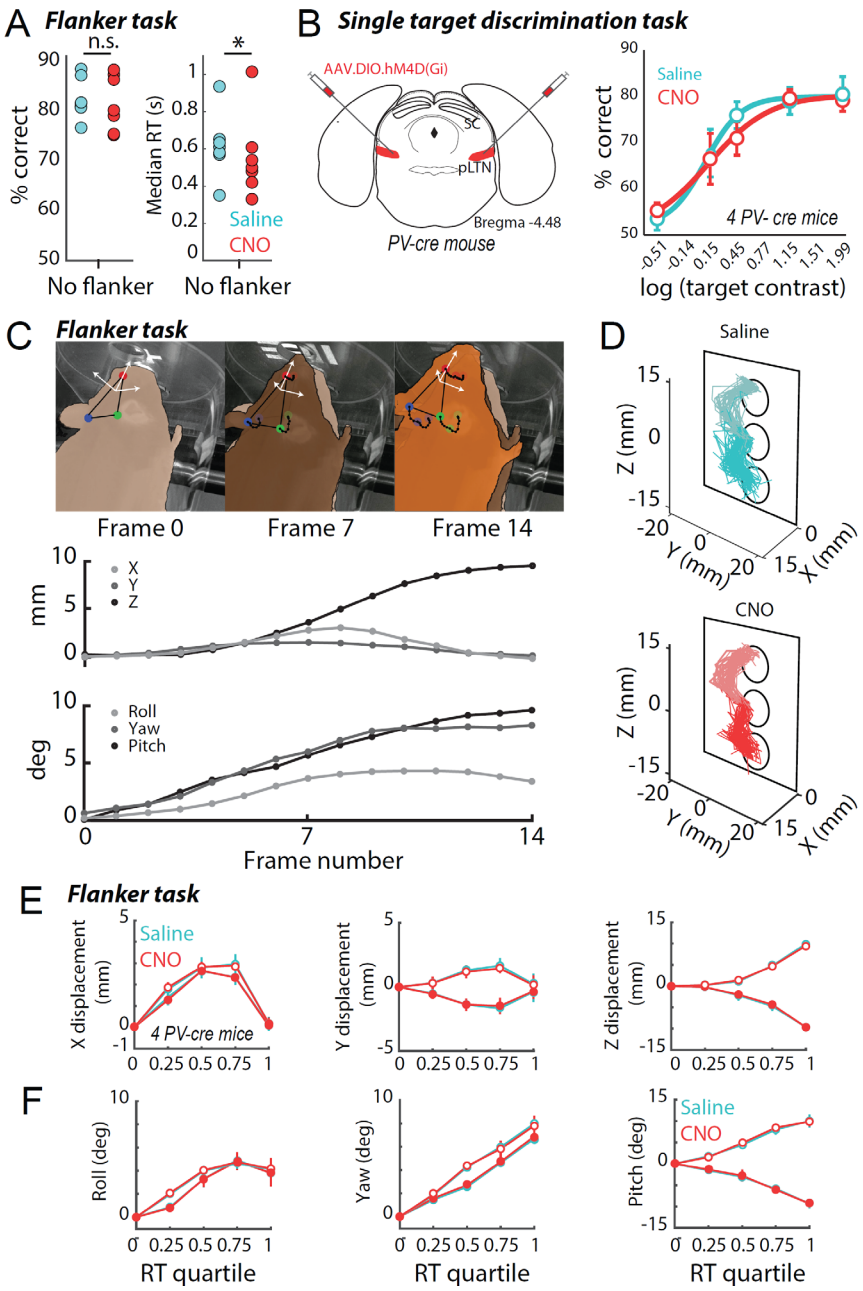

Fig. 4. Bilateral pLTN inactivation does not affect visual perception of single targets or motor orienting. (A) *Comparison of task parameters across the saline and CNO conditions for congruent and incongruent task conditions for 7 PV-Cre mice. (Left) Mean percentage correct, (right) Median RT. Each dot represents data from one mouse.* ***(B)*** *Performance for discrimination task across Saline and CNO conditions for 4 PV-Cre mice. (left) Schematic showing location of bilateral inhibitory DREADDs injection in the pLTN. (right) Percentage correct across five target contrasts for saline (open cyan circles, mean +/- sem) and CNO (open red circles, mean +/-sem). Corresponding solid lines are sigmoid fits.* ***(C)*** *(top) Snapshots of mouse movements in an example up nose-poke choice trial, across frames. Red, blue and green filled circles on mouse head indicate labels generated by the automated deeplearning tracking tool (see Methods). Black dotted lines indicate movement trajectories across all tracked frames. White arrows indicate the egocentric coordinate axis constructed using the three labeled markers. (middle) X,Y and Z coordinates of tracked nasal point (red filled circle in snapshots). (bottom) Constructed roll, yaw and pitch values in example trial.* ***(D)*** *Reconstructed head movement trajectories across saline (top, cyan) and CNO (bottom, red) for all trials for an example session. Lighter colors indicated trials in which mouse nose-poked the top port. Black rectangle and circles show the nose-poke mask used in the behavioral apparatus (Fig.*

*3A,B). **(E)** Comparison of X (left), Y (middle) and Z (right) displacement (mean +/- sem) for the Flanker Task across Saline (cyan) and CNO (red) conditions for 4 PV-Cre mice across RT quartiles. Open circles, up nose-poke trials. Closed circles down nose-poke trials. **(F)** similar to E, but for roll, yaw and pitch across RT quartiles.*

DISCUSSION

This study discovers the necessity of pLTN, a group of PV+ inhibitory neurons in the midbrain, for accurate and reliable target selection for selective spatial attention. Our results demonstrate that pLTN disrupts attentional control in a competitive setting by disrupting distracter suppression without affecting the perceptual sensitivity of single targets or orienting behavior (unlike the functions of the midbrain superior colliculus or the prefrontal cortex; (*5, 29*). We propose, therefore, that the evolutionarily conserved pLTN is a midbrain engine dedicated to resolving stimulus competition and target selection for spatial attention.

A potential mechanism by which pLTN controls selective spatial attention is revealed by our electrophysiological results (Fig. 2) - namely pLTN's action at the sensorimotor hub, the SCid. Considering that the SCid is itself required for spatial attention control (refs), the leftward shift of the competitive-strength dependent response profiles in SCid following bilateral pLTN inactivation (Fig. 2C, 2E-left) is predictive of the leftward shift of the psychometric response profile (of accuracy) in the flanker task following bilateral pLTN inactivation (Fig. 3J). Similarly, the loss of categorical signaling of the strongest stimulus by SCid (Fig. 2C, 2E-right) is predictive of the loss of reliable behavioral signaling of the highest priority attentional target during the flanker task (Fig. 3J; we note that the top-down expectation of the target's location and its physical salience, together constituting the target's priority, compete against the flanker's salience in the battle for control of the attentional locus in the flanker task). Finally, the significant overall increase (upward shift) in SCid response rates following bilateral pLTN inactivation (Fig. 2CD) is predictive of the faster reaction times in the flanker task following bilateral pLTN inactivation (Fig. 3H-right; consistent with SC's role in primates; (*31, 32*). Together, these results suggest the scenario of pLTN being the midbrain site that implements distracter suppression and competitive selection of the highest priority stimulus, shaping SCid relative priority map, which, in turn, drives attentional behavior.

Selective silencing of just the pLTN projections in SCid would allow a direct test of this hypothesis that pLTN acts at the SCid in order to exert behavioral control of selective spatial attention. Separately, bilateral chemogenetic inactivation of pLTN, as performed here, allowed SC to continue to exhibit residual stimulus competition reflecting signals of competition from descending fronto-parietal inputs. By contrast, spatially focal pLTN silencing would allow testing of whether pLTN is the exclusive source of long-range competitive inhibition in the mammalian SCid (as in birds, (*9*)), or if it is only one of a few such sources (including potentially long-range intra- and inter-collicular inhibition – (*33-35*)). Finally, detailed anatomical tracing coupled with functional and behavioral experiments would allow testing of whether self-sparing ('donut-like') connectivity exists between the pLTN and SC (as in non-mammals, (*14, 22, 23*), and whether it controls categorical signaling by SC (as demonstrated recently in birds; (*22*)), and as well, categorical selection behavior. All of these represent fruitful future directions for dissecting the functional logic of the evolutionarily ancient pLTN's role in spatial attention control. The current study, therefore, establishes a critical first step in accessing a detailed mechanistic picture for the control and dysfunction of selective spatial attention.

Acknowledgments: We thank Sarah Correas, Samrawit Getachew, Isabel Rios Pulgar, Sarah Saccal, and Ronald Salazar for help with behavioral training of the mice, and Spencer Loggia and Ntumba Loic Sangwa, for help with the cameras.

Funding: This work was supported by NIH F32EY032776 (NBK), NIH R34NS111653 (SPM), NSF 2047298 (CAREER award, SPM) and start-up funds from the Johns Hopkins University (SPM).

Author contributions: SPM and NBK conceived the project and designed the experiments; NBK performed and supervised behavioral experiments and data analyses; NBK and QZ performed the electrophysiological experiments and analyses; WKY, AB and NBK performed anatomical experiments and analyses; SPM and NBK wrote the paper.

Competing interests: The authors declare that they have no competing interests.

Data and materials availability: Code, data and materials used in the analysis will be made available upon reasonable request to the corresponding author.

MATERIALS AND METHODS

Animals

For behavior and electrophysiological studies, adult (8+ weeks old; equal male and female) wildtype mice (C57Bl6/J strain, Jackson Laboratory), and PV-Cre (homozygous, Jackson Laboratories, Stock #017320) mice were used. For parvalbumin (PV) and GABA immunohistochemistry studies, adult (8+ week old, male C57BL6J mice (Jackson Laboratory) were used. For tracing SC input to pLTN, PV-tdTomato mice (adult, Jackson Labs) reporter mice were used and for tracking pLTN projections to SC, PV-Cre mice were used. Upon arrival, all mice were housed in a colony where temperature (~75° F) and humidity (~55%) were controlled on a 12:12 h light:dark cycle, and all procedures were performed after allowing mice to acclimatize for at least 7 days in the new environment. All procedures followed the NIH guidelines and were approved by the Johns Hopkins University Animal Care and Use Committee.

Stereotactic Surgery

Animals were anesthetized with isoflurane (3% induction, 0.5–2% maintenance) and were secured by a stereotaxic frame with ear bars (Kopf Instruments). A feedback-controlled heating pad (FHC) was used to maintain the body temperature at 36.8°C, and artificial tears were applied to the eyes to prevent them from drying. After the head of the animal was leveled in the stereotaxic frame, fur was shaved off above the animal's skull, exposed skin was cleaned using betadine (antiseptic) using sterile wipes and bupivacaine was injected subcutaneously for perioperative analgesia. A scalp incision was made along the midline, followed by muscle retraction and cleaning. Once bregma and lambda were exposed, the skull was zeroed using the Kopf stereotax. For bilateral pLTN inactivation, craniotomies were made for virus injection (AP -4.4; ML +/-1.65; DV -3.3 from Bregma, AAV8.DIO.hM4D(Gi), Addgene catalog #44362). For head-fixed electrophysiology studies (with bilateral pLTN inactivation) an additional craniotomy was made above the SC (AP -3.5; ML +/-0.9). All coordinates are based on a standard mouse brain atlas (Franklin and Paxinos, 2008). Each mouse was injected with 300 nl of virus at each site, at a flow rate of 0.3 nl/s, using a 2 μL Hamilton syringe (7002, Catalog #88400) using a pressure microinjector (Harvard Instruments). Craniotomies were covered with KwikSil (World Precision Instruments) for protection. For behavior only studies and anatomical tracing studies, skin was sutured using tissue adhesive (Loctite, #4013). For mice used in recording SC visual responses (with bilateral pLTN inactivation), a custom-made titanium headbolt was stereotactically affixed to skull using Metabond (Parkell) and the bregma location was kept exposed. Dexamethasone was administered to reduce inflammation. After surgery, mice received meloxicam injections daily for up to 3d to ease discomfort.

Immunohistochemistry

Mice were deeply anesthetized with intraperitoneal injection of pentobarbital-based euthanasia solution (250 mg/kg body weight) and transcardially perfused with 1M phosphate buffered saline (PBS) followed by 4% paraformaldehyde (PFA). Brains were removed from the skull, postfixed in 4% PFA at 4°C for 24 hours, then transferred to a solution of 30% sucrose in 4% PFA at 4°C for another 36 hours. Coronal sections (50 μm thickness) were obtained using a cryostat (Leica Microsystems, model CM-1860). Free floating sections were washed three times in PBS (10 minutes each) and then incubated in a blocking solution containing 10% normal goat serum (NGS, Abcam #ab7481), 0.5% Triton X-100 in PBS for 2 hours at room temperature on a shaker. Sections were then incubated in a solution containing the primary antibody, 10% NGS, 0.5% Triton X-100 in PBS for 72 hours at 4°C, with occasional shaking. The following primary antibodies were used: (1) rabbit anti-gamma amino butyric acid (GABA; Sigma-Aldrich #A2052, 1:1000 dilution) (2) rabbit anti-parvalbumin (PV; Abcam #ab11427, 1:500 dilution). The sections were then rinsed thrice with PBS and incubated in a solution containing secondary antibodies, 10% NGS, 0.5% Triton X-100 in PBS for 3-5 hours at room temperature, with occasional shaking. The following secondary antibodies were used: AlexaFluor 488 (Abcam) for GABA (dilution 1:500) and AlexaFluor 555 (Abcam) for PV (dilution 1:200). Sections were washed thrice with PBS and mounted onto slides with DAPI fluoromount-G (SouthernBiotech, #0100-20) and protected with coverslips.

Microscopy and Data Analysis

Fluorescent images of double immunolabeled neurons were obtained using a Zeiss laser scanning confocal microscope (LSM 700). Z-stacked images from the pLTN area were obtained using a 40x objective oil immersion lens, with a screen resolution of 1024×1024 pixels and a step size of 0.5 microns. For quantification, images were z-projected with maximum intensity and the number of stained cell bodies were identified over a 160μm × 160μm unit area. Cell bodies were identified, separately for PV and GABA from the same sections. The number of overlapping cell bodies were then calculated using a custom MATLAB script.

Head-fixed experiments

Following surgery chemogenetic virus was allowed to express for 3+ weeks, which also gave mice (adult PV-Cre mice) enough time to recover from effects of surgery.

Apparatus. Mice were head-fixed in a custom setup, with their bodies resting comfortably on a hammock, and their heads facing a screen (Viotek 32 inch LED monitor) directly in front, providing a viewing angle of +/- 35° elevation and +/- 55° azimuth. The head-fixing mechanism allowed mice to be held in the zeroed position determined during surgery, allowing precise placement of electrode in the brain. Electrodes for extracellular electrophysiological recordings were held in a custom-made holder with micromanipulator stages for movement in X, Y (manual) and Z (motorized – Newport, 0.1 um accuracy) directions. To reduce acoustic interference during recordings, the entire setup was placed in a custom-made sound attenuation chamber.

Electrophysiology. All recordings were made using acute single shank 32-ch silicon probes (Neuronexus, 0.3 – 1.5MΩ at 1 kHz). Electrodes were first zeroed at the exposed bregma location (see Materials and Methods, surgical techniques) and then stereotactically lowered onto the SC surface. Extracellular recordings were made from single and multiunit sites in the intermediate and deep layers of the SC (SCid), with the probe position based on the standard mouse brain atlas (Franklin and Paxinos, 2008). Neural activity synchronized with visual stimulus presentation times was collected via a 32 channel headstage (Intan technologies), was sampled at 30 kHz and stored on a PC using a data acquisition system (OpenEphys).

Visual stimuli. Visual stimuli were created using customized MATLAB software (Schryver et al, 2020, Mahajan and Mysore, 2022). Once head-fixed, the mouse was held in the zeroed position such that the midline (visual axes) were in the horizontal plane aligned with 0° elevation and 0° azimuth of the screen. Looming stimuli were constructed as previously reported in Mysore et al, 2010. Briefly, looming visual stimuli consisted of a black dot on a gray background that

progressively increased in size over the period of stimulus presentation (500 ms) starting from a size of 1.25° radius. The center of a looming stimulus remained constant throughout the duration of the motion stimulus. Loom speed was defined as the rate of change of the angular size of the dot, $d\theta/dt$, where θ is the visual half-angle subtended by the object at the eye.

The competing stimuli used in this study is based on Mysore et al, 2011. Briefly, two looming stimuli were simultaneously presented (Fig 3C): one stimulus, S_{in}, was presented inside the receptive field of the unit and its strength was held constant, whereas the second stimulus, S_{out}, was presented outside the receptive field and its strength was systematically varied. The resulting responses from this protocol were collectively referred to as a competitor strength–response profile (CRP). The S_{in} stimulus location (and receptive fields) were chosen to be in the front-central and binocular region of the visual field (within 15°-0° azimuthal in left hemifield, and +/-10° elevation), to ensure that the S_{in} stimulus location (on the screen) overlapped with the spatial location of the target stimulus in the behavioral experiments (see Materials and Methods: Behavior). For most sites spatial tuning of the S_{in} stimulus was only coarsely estimated (by hand). The S_{out} stimulus was presented on the contralateral side, outside, 30° away from the center of the S_{in} receptive field (S_{out} located between 25° and 40° away in azimuth and between 0° and 10° away in elevation). When possible, it was ensured that the S_{out} stimulus location (on the screen) overlapped with the spatial location of the Flanker stimulus in the behavioral experiments (see Materials and Methods: Behavior). The strength of the looming S_{out} stimulus was varied across the range of 0 –24°/s in eight equal steps. We determined this to be the range of loom speeds over which SCid neurons are most sensitive. Out of the eight loom speed strengths, S_{in} was chosen to be near the 5th strength level.

Experimental protocol and data collection. After baseline (saline or no-saline) competitor-response-profile data collection, the mouse was subcutaneously administered CNO (Tocris) to bilaterally inactivate the pLTN. After 30 minutes, CRP data was collected again. We found no difference between the baseline and saline CRP data. In separate sessions, we confirmed the inactivation of pLTN, by recording spontaneous as well as visually evoked activity, before and after CNO administration. Further, to functionally test the spread of the virus, we used a 4-shank silicon probe (NNX – probe #) with one shank stereotactically placed in the pLTN and 3 shanks outside, we confirmed that CNO administration had no effect on spontaneous activity at locations outside the pLTN.

Data analysis. All analyses were performed with custom MATLAB code. Response firing rates were computed by counting spikes over an approximately 250 ms long window with respect to stimulus onset, and converting the resulting count into spikes per second. Best sigmoidal fits to CRPs were obtained by using a nonlinear least squares estimation procedure (*nlinfit* command in MATLAB) (Mysore et al, 2011). The transition range of a CRP was defined as the range of S_{out} loom speeds over which responses dropped from 90 to 10% of the total range of responses. The switch value for switch-like CRPs was defined as the strength of the S_{out} stimulus at which responses to the paired stimuli changed abruptly from high to low, and was numerically estimated as the midpoint of the transition range of the CRP. Categorization index of the competitor strength-dependent response profile was calculated per previously published work (Mysore and Knudsen, 2011).

Behavior

Apparatus. Behavioral training and testing were performed in soundproof operant chambers equipped with a touchscreen (K-Limbic, and Med-Associates Inc.). A reward port (fluid well) was located at the wall opposite to the touchscreen (Fig. 3A). The operant chamber was also equipped with a house light for delivering negative reinforcement on error trials. Two high-speed infrared video cameras (FLIR, BlackFly) were used to record head movements around the touchscreen. During the training, to minimize exploratory behavior and to ensure task focus, mice were placed in a plexiglass tube (5 cm diameter) which allowed enough space for free movement. Further, a plexiglass mask with three vertically placed nose-poke holes (Fig. 3A, 3B) prevented mice from

gaining direct access to the touchscreen. These three nose-poke holes were the only locations through which the mouse could interact with the screen (center hole – trial initiation; top and bottom – to indicate choice) (Fig. 3A and 3B). Timing of stimulus presentation, water and sound delivery were controlled using a custom software (K-Limbic v1.30, Med Associates).

Visual stimuli. Visual stimuli used for the visuospatial attention task were the same as previously published (You and Mysore, 2020). Briefly, visual stimuli (bright objects on a dark background; background luminance = 1.32 cd/m2) were generated using MATLAB (Mathworks). All stimuli were small, of size 60 pixels × 60 pixels, i.e., 12mm × 12 mm, and subtended a visual angle of 25° at a viewing distance of 20mm from the mask. A zeroing cross (luminance = 130 cd/m2, Figure 3B) was presented in the central hole and had to be touched to initiate each trial. The experimental stimuli were oriented gratings (horizontal or vertical orientation), generated using a square wave of spatial frequency 24 pixels/cycle (0.1 cycles per degree). Contrast of the gratings was defined as the ratio of difference in luminance between the bright and dark phases of the grating over that of the dark phase: contrast = (Lbright – Ldark)/Ldark (units of fractional change).

Experimental procedure and behavioral training. Each mouse was run for one 30-min behavioral session per day, with each session yielding typically, 120–180 trials. Mice were trained to initiate trials by nose-poking the zeroing cross which appeared at the central hole. Upon trial initiation, the cross vanished, and the visual stimulus (or stimuli) were immediately presented for a duration of 2s depending on the task (see below). Mice were trained to report the information contained in the target grating, namely, its orientation, by nose-touching within the correct response hole (For example, vertical target grating → nose-touch in top response hole; horizontal target grating → nose-touch in the bottom response hole). Response choices were counterbalanced across mice. A correct response triggered a tone (600 Hz, 1 sec) and the delivery of 10 µL of water at the reward port. Mouse head entry into the reward port was detected by an infrared sensor which caused the magazine light to turn off, and the zeroing cross (for the next trial) to be presented on the touchscreen. An incorrect response triggered the turning on of the house light for 5 s as a timeout; the next trial could not be initiated until the end of timeout. A failure to respond within 3 s of stimulus presentation resulted in the stimulus vanishing and the zeroing cross being presented immediately (without a timeout penalty) for initiation of the next trial. These trials are counted as missed trials. Well-trained animals failed to respond on fewer than 5% of the total number of trials, and there were no systematic differences in the proportion of such missed trials between different conditions. Within each daily 30-min behavioral session, mice consumed ~1 mL of water. If a mouse failed to collect enough water from the behavioral session, they were provided with a water supplement using a small plastic dish in their home cage. The specific amount of supplement was customized depending on individual animal's body weight, the training phase it was in, and the motivational drive observed during the experiment.

Discrimination task (single stimulus). Upon trial initiation, a single, full contrast, grating stimulus (target, contrast = 14.2; size = 60 × 60 pixels2, 25°, 2.5 cycles, Fig. 4A) was presented above the central hole, aligned along the elevation with the left and right holes. The stimulus was presented for a duration of 2 s, and mice were required to report its orientation with the appropriate nose-touch within 3 seconds.

Flanker task. Upon trial initiation, either one stimulus (target, 60 × 60 pixels2, 25°, 2.5 cycle, 1 s, contrast = 14.2, Fig. 3B) was presented at the central location, or two stimuli were presented simultaneously, with the target at the central location and a second stimulus (flanker) at the left of the target location. Thus, the task consisted of three main conditions, 1. *target only condition*, where no flanker was present, 2. *congruent only condition*, where the flanker had the same orientation as the target and 3. *incongruent flanker condition*, where the flanker had the opposite orientation as the target. The target contrast was always kept constant. Flankers were of the same size and spatial frequency as the target, but with contrasts at 8 different levels: 0.31, 0.73, 1.42, 2.79, 5.84, 14.2, 34.4, and 97.5. All 17 stimulus conditions were interleaved randomly. The stimuli were presented for a duration of 2 s, and mice were required to report orientation of the target grating with the appropriate nose-touch within 3 s (Fig. 3A). All types of trials (no flanker,

congruent, incongruent) and flanker contrasts were interleaved randomly within each daily session. Mice were first trained on the discrimination task, following which, a flanker was introduced on the left with progressively increasing contrast over training days.

Chemogenetic inactivation

To reduce stress induced due to handling and administration of intraperitoneal injections, 2 weeks prior to the start of experiments, mice were handled daily for 2-3 minutes, about 30 minutes before each training session. Gradually mice were subject to being gently scruffed and once they were accustomed to handling and scruffing, saline i.p. injections were administered. Once mice had been administered i.p. injections for 3 consecutive days, data collection commenced. On data collection days, the previously established routine of handling, scruffing and i.p. injections (Saline or CNO), 30 minutes prior to data collection, was followed. Saline and CNO (Tocris, final concentration 5 mg/kg) experimental sessions were run in blocks. Blocks were counter-balanced across mice.

Analysis of behavior data

Behavioral data collection and measurements. Task related event information such as trial initiation time, choice report time and direction of choice report were synced and stored on a PC by the K-limbic software. This information was used post-hoc to calculate response accuracy (% correct – the number of correct trials divided by the total number of trials responded, reaction time (RT - defined as the time between the start of stimulus presentation and response nose-touch.

Calculation of perceptual sensitivity. Using methods from signal detection theory, we assigned the correct vertical trials as “hits”, incorrect vertical trials as “misses”, correct horizontal trials as “correct rejections”, and incorrect horizontal trials as “false alarms”, and calculated the perceptual sensitivity (d’). Data for saline and CNO sessions were separately analyzed.

3D head-tracking. Daily before each experimental session, a volume of space (5x5x5 cm^3) around the nose-poke mask (Fig. 3A) was calibrated using a 20x20 checkerboard stimulus, and by collecting 1000 frames of synchronized videos on each camera. Post-hoc the points on the checkerboard in the calibration videos were detected and assigned using a custom-made automated script in Matlab. Using the labeled checkerboard points the cameras were calibrated using MagicWand (*36*) Matlab based software.

For each mouse, three points on the head were labeled using a deep-learning based tool (dltdv8 – (*36*)), which used the camera calibration data to generate labeled trajectories (x,y and z coordinates) in 3D space. For each trial the frames from trial initiation (nose-poke at center hole – Fig. 3B, 4CD) till choice report (nose-poke at the top or bottom holes – Fig. 3B, 4CD) were labeled. Videos were labeled for four mice for both Saline and CNO conditions. The labeled points were rotated and shifted to a co-ordinate axes with origin at the center of the middle nose-poke hole. Using the three points, roll, yaw and pitch were calculated. To allow comparisons across variable trials times, head-trajectories were plotted in X, Y and Z co-ordinates, as well as roll, yaw and pitch angles, by RT quantiles and compared across conditions (Fig. 4EF).

Statistical analyses.

All analyses and statistical tests were performed in MATLAB. The stated P-values were computed using the non-parametric Wilcoxon signed-rank test (two-tailed) was used to test if the median of the distribution of the change in the metric between conditions (e.g., Saline vs CNO) was different from zero. Where corrections for multiple comparisons were required (as stated in the text), these were performed using the Holm–Bonferroni test for multiple comparisons (unless other stated). Statistical significance was defined as $p < 0.05$. No power analysis was performed to predetermine sample size, but our sample sizes are similar to those

generally employed in the field. All data are presented as mean ± standard error of the mean (SEM), unless otherwise noted.

REFERENCES

1. J. H. Fecteau, D. P. Munoz, Salience, relevance, and firing: a priority map for target selection. *Trends Cogn Sci* **10**, 382-390 (2006).
2. E. I. Knudsen, Fundamental components of attention. *Annu Rev Neurosci* **30**, 57-78 (2007).
3. E. I. Knudsen, Control from below: the role of a midbrain network in spatial attention. *Eur J Neurosci* **33**, 1961-1972 (2011).
4. R. J. Krauzlis, L. P. Lovejoy, A. Zenon, Superior colliculus and visual spatial attention. *Annu Rev Neurosci* **36**, 165-182 (2013).
5. L. P. Lovejoy, R. J. Krauzlis, Inactivation of primate superior colliculus impairs covert selection of signals for perceptual judgments. *Nat Neurosci* **13**, 261-266 (2010).
6. R. M. McPeek, E. L. Keller, Deficits in saccade target selection after inactivation of superior colliculus. *Nat Neurosci* **7**, 757-763 (2004).
7. R. H. Wurtz, J. E. Albano, Visual-motor function of the primate superior colliculus. *Annu Rev Neurosci* **3**, 189-226 (1980).
8. S. P. Mysore, E. I. Knudsen, The role of a midbrain network in competitive stimulus selection. *Curr Opin Neurobiol* **21**, 653-660 (2011).
9. S. P. Mysore, E. I. Knudsen, A shared inhibitory circuit for both exogenous and endogenous control of stimulus selection. *Nat Neurosci* **16**, 473-478 (2013).
10. A. M. Graybiel, A satellite system of the superior colliculus: the parabigeminal nucleus and its projections to the superficial collicular layers. *Brain Research* **145**, 365-374 (1978).
11. A. R. Harvey, D. R. Worthington, The projection from different visual cortical areas to the rat superior colliculus. *The Journal of Comparative Neurology* **298**, 281-292 (1990).
12. Z. D. Jiang, D. R. Moore, A. J. King, Sources of subcortical projections to the superior colliculus in the ferret. *Brain Res* **755**, 279-292 (1997).
13. R. J. Krauzlis, A. R. Bogadhi, J. P. Herman, A. Bollimunta, Selective attention without a neocortex. *Cortex*, 1-15 (2017).
14. M. I. Sereno, P. S. Ulinski, Caudal topographic nucleus isthmi and the rostral nontopographic nucleus isthmi in the turtle, Pseudemys scripta. *J Comp Neurol* **261**, 319-346 (1987).
15. G. Paxinos, K. B. Franklin, *Paxinos and Franklin's the mouse brain in stereotaxic coordinates*. (Academic press, 2019).
16. M. A. Basso, M. E. Bickford, J. Cang, Unraveling circuits of visual perception and cognition through the superior colliculus. *Neuron* **109**, 918-937 (2021).
17. Z. D. Jiang, A. J. King, D. R. Moore, Topographic organization of projection from the parabigeminal nucleus to the superior colliculus in the ferret revealed with fluorescent latex microspheres. *Brain Research* **743**, 217-232 (1996).
18. G. Marin *et al.*, A cholinergic gating mechanism controlled by competitive interactions in the optic tectum of the pigeon. *J Neurosci* **27**, 8112-8121 (2007).
19. S. P. Mysore, A. Asadollahi, E. I. Knudsen, Signaling of the strongest stimulus in the owl optic tectum. *J Neurosci* **31**, 5186-5196 (2011).
20. S. P. Mysore, E. I. Knudsen, Descending control of neural bias and selectivity in a spatial attention network: rules and mechanisms. *Neuron* **84**, 214-226 (2014).

21. A. Asadollahi, S. P. Mysore, E. I. Knudsen, Stimulus-driven competition in a cholinergic midbrain nucleus. *Nat Neurosci* **13**, 889-895 (2010).
22. N. R. Mahajan, S. P. Mysore, Donut-like organization of inhibition underlies categorical neural responses in the midbrain. *Nat Commun* **13**, 1680 (2022).
23. Y. Wang, D. E. Major, H. J. Karten, Morphology and connections of nucleus isthmi pars magnocellularis in chicks (Gallus gallus). *J Comp Neurol* **469**, 275-297 (2004).
24. W. K. You, S. P. Mysore, Endogenous and exogenous control of visuospatial selective attention in freely behaving mice. *Nat Commun* **11**, 1986 (2020).
25. B. A. Eriksen, C. W. Eriksen, Effects of noise letters upon the identification of a target letter in a nonsearch task. *Perception & Psychophysics* **16**, 143-149 (1974).
26. J. Fan, B. D. McCandliss, T. Sommer, A. Raz, M. I. Posner, Testing the efficiency and independence of attentional networks. *J Cogn Neurosci* **14**, 340-347 (2002).
27. D. G. Pelli, M. Palomares, N. J. Majaj, Crowding is unlike ordinary masking: distinguishing feature integration from detection. *J Vis* **4**, 1136-1169 (2004).
28. S. T. Chung, D. M. Levi, G. E. Legge, Spatial-frequency and contrast properties of crowding. *Vision Res* **41**, 1833-1850 (2001).
29. A. Bollimunta, A. R. Bogadhi, R. J. Krauzlis, Comparing frontal eye field and superior colliculus contributions to covert spatial attention. *Nat Commun* **9**, 3553 (2018).
30. A. F. Meyer, J. O'Keefe, J. Poort, Two Distinct Types of Eye-Head Coupling in Freely Moving Mice. *Curr Biol* **30**, 2116-2130 e2116 (2020).
31. T. B. Crapse, H. Lau, M. A. Basso, A Role for the Superior Colliculus in Decision Criteria. *Neuron* **97**, 181-194.e186 (2018).
32. J. P. Herman, L. N. Katz, R. J. Krauzlis, Midbrain activity can explain perceptual decisions during an attention task. *Nat Neurosci* **21**, 1651-1655 (2018).
33. J. Essig, J. B. Hunt, G. Felsen, Inhibitory neurons in the superior colliculus mediate selection of spatially-directed movements. *Commun Biol* **4**, 719 (2021).
34. R. Huda, M. J. Goard, G. N. Pho, M. Sur, Neural mechanisms of sensorimotor transformation and action selection. *Eur J Neurosci* **49**, 1055-1060 (2019).
35. T. Isa, in *Current opinion in neurobiology*. (2002), vol. 12, pp. 668-677.
36. D. H. Theriault *et al.*, A protocol and calibration method for accurate multi-camera field videography. *Journal of Experimental Biology* **217**, 1843-1848 (2014).